# DEVELOPMENT OF A FATIGUE CRACK GROWTH COUPON FOR HIGHLY PLASTIC STRESS CONDITIONS

Phillip A. Allen*, Pravin K. Aggarwal†, and Gregory R. Swanson‡
NASA Marshall Space Flight Center
Huntsville, AL
phillip.a.allen@nasa.gov

## ABSTRACT

The analytical approach used to develop a novel fatigue crack growth coupon for highly plastic stress field condition is presented in this paper. The flight hardware investigated is a large separation bolt that has a deep notch, which produces a large plastic zone at the notch root when highly loaded. Four test specimen configurations are analyzed in an attempt to match the elastic-plastic stress field and crack constraint conditions present in the separation bolt. Elastic-plastic finite element analysis is used to compare the stress fields and critical fracture parameters. Of the four test specimens analyzed, the modified double-edge notch tension - 3 (MDENT-3) most closely approximates the stress field, *J* values, and crack constraint conditions found in the flight hardware. The MDENT-3 is also most insensitive to load misalignment and/or load redistribution during crack growth.

## INTRODUCTION

This paper presents the analytical approach used to develop a novel fatigue crack growth coupon for a highly plastic three-dimensional (3-D) stress field condition. The flight hardware investigated in this paper is a large separation bolt that fractures using pyrotechnics at the appointed time during the flight sequence. The separation bolt has a deep notch that produces a severe stress concentration and a large plastic zone when highly loaded. For this geometry, linear-elastic fracture mechanics (LEFM) techniques are not valid due to the large nonlinear stress field at the notch root. Unfortunately, industry codes that are commonly available for fracture mechanics analysis and fatigue crack growth (e.g. NASGRO[1]) are generally limited to LEFM and are available for only a limited number of geometries. The results of LEFM based codes are questionable when used on geometries with significant plasticity. Therefore elastic-plastic fracture mechanics (EPFM) techniques using the finite element method were used to analyze the separation bolt.

A testing program was developed to verify the EPFM separation bolt analysis results. Testing of full-scale flight hardware is very costly in terms of assets, laboratory resources, and schedule. Therefore to alleviate some of these problems, a series of novel test specimens were developed to simulate the elastic-plastic stress field present in the bolt. Finite element models were created to predict the stress fields in the test specimens and the flight hardware. In addition, finite element models of cracked test specimens and flight hardware were created to compare critical fracture parameters along the crack front. A summary of the test specimen geometry development is given below.

## SPECIMEN GEOMETRY DEVELOPMENT

### Notched Plate Specimen

The first test coupon developed was the notched plate (NP) specimen as shown in Figure 1-(a). The gage section of the NP matches the cross sectional dimensions of the notch region of the separation bolt. The specimen is pin loaded on a narrow land (0.20 in. wide) in the center of the pin holes to help ensure load alignment. Unfortunately this specimen design is very sensitive to load placement, and, therefore, a small change in load alignment results in widely varying stress fields in the notch region

### Modified Double-Edge Notch Tension Specimens

To reduce the alignment sensitivity of the specimen, a modified double-edge notch tension (MDENT) specimen was developed (Figure 1-(b)). This specimen has the advantage of being symmetric, which reduces bending sensitivity, while still preserving the free surface on the back face of the notch section. This specimen was an improvement over the NP specimen, but was still relatively sensitive to load alignment due to the stiffness of the transition section below the pin hole.

To reduce the alignment sensitivity of the specimen even more, the distance between the two notch sections was increased and fillets were cut into the transition section below the pin holes. Using two different transition fillet radii resulted in the MDENT-2 (Figure 1-(c)) and MDENT-3 (Figure 1-(d)) specimens. The moment of inertia, *I*, for the fillet section on MDENT-2 is approximately 53% that of the notched section, and *I* for the fillet section on MDENT-3 is approximately 8% of that of the notched section. For misaligned loads, the thin fillet section acts as a flexure and therefore helps preserve the desired stress state in the notch sections.

---

* Structural Analyst, Strength Analysis Group/ED22, NASA/MSFC
† AIAA Member, Deputy Group Lead - Strength Analysis Group/ED22, NASA/MSFC
‡ Structural Analyst, Strength Analysis Group/ED22, NASA/MSFC

## MATERIAL PROPERTIES

The separation bolt housing is made of 4340 steel. Material properties for 4340 were obtained from uniaxial tensile tests performed at Marshall Space Flight Center (MSFC). A summary of the general material properties for 4340 steel is shown in Table 1. Elastic-plastic finite element analysis using the commercial finite element code ABAQUS[2] requires a table of true stress versus plastic strain, $\varepsilon^{pl}$. Therefore, $\sigma$ and $\varepsilon^{pl}$ values were calculated from the uniaxial tensile data and used as inputs for the von Mises plasticity model in ABAQUS. Data points from the actual test record were used for the initial portion of the table values. After the maximum load, the test record no longer represents a uniaxial stress-strain response due to necking of the test specimen. Therefore, an additional point at $\varepsilon^{pl} = 1.0$ and $\sigma = 210$ kip was added to the end of the data to complete the table and to ensure stability in the plasticity solution algorithm. A plot of the ABAQUS plasticity inputs compared to the $\sigma$ versus $\varepsilon^{pl}$ tensile test data is shown in Figure 2.

## FINITE ELEMENT MODELING

### Separation Bolt Finite Element Models

#### Axisymmetric Finite Element Model

An axisymmetric finite element model (FEM) of a portion of the separation bolt was developed to determine the stress fields in an un-cracked bolt. The axisymmetric FEM was created by utilizing the axis of symmetry along the longitudinal axis of the bolt and the symmetry plane passing through the notch root as shown in Figure 3. The finite element mesh and boundary conditions were created using PATRAN[3], and the FEM was analyzed and post-processed using ABAQUS[2]. The FEM was composed of 566 4-node reduced integration axisymmetric elements (type CAX4R in ABAQUS) and has 626 nodes. A uniform pressure was applied to the top nodes of the FEM for the loading boundary condition.

#### 3-D Finite Element Model with Crack

A multi-step process was used to create the 3-D finite element model of the separation bolt with a crack in the base of the notch as shown in Figure 4. First, a 3-D, one-eighth FEM of the bolt was created in PATRAN. This FEM was created by utilizing three symmetry planes: one plane through the center of the notch and two additional planes 90° apart through the longitudinal axis. The FEM was composed of 20-node reduced integration bricks (type C3D20R in ABAQUS). A small volume of elements was then removed from the bolt FEM to create a "crack-block" definition mesh. The crack-block geometry was then read into a commercial crack mesh generation code, FEA-Crack[4]. The crack mesh was created using FEA-Crack, and an ABAQUS input file was output for the crack mesh and associated boundary conditions. An ABAQUS input file for the "master" FEM of the bolt minus the crack-block was then created using PATRAN. The crack mesh input file and the master bolt input file were then manually combined into one ABAQUS input file using a text editor. The two dissimilar meshes were joined using the "*TIE" command in ABAQUS for tied contact. The final 3-D fem with crack was composed of 5,804 elements and 27,204 nodes. A uniform pressure was applied to the top surface of the FEM for the loading boundary condition, and the FEM's were analyzed and post-processed using ABAQUS.

The crack-front mesh consists of 20-node reduced integration bricks that have one collapsed face and midside nodes moved to the quarter-points (see Figure 5). The elements are modified in this way to create a singular stress field at the crack front. This modification results in 3 nodes collapsed to the same location at the element edges and 2 nodes collapsed to the same location at the element midplane along the collapsed side. For an elastic-plastic analysis, the collapsed nodes are allowed to displace independently, allowing the crack tip to "blunt." The sets of collapsed nodes define the geometry of the crack front in ABAQUS and are used as inputs in the "*CONTOUR INTEGRAL" command to calculate the $J$-integral values along the crack front.[2]

### Notched Plate Finite Element Model

A 3-D FEM of the notched plate specimen was created using 6,384 20-node reduced integration bricks and 29,783 nodes as shown in Figure 6. Two symmetry planes were utilized in creating the FEM by dividing the geometry along the longitudinal axis and along the center of the notch root. A concentrated force was applied to a node or nodes along the top of the "pin hole" to simulate centered or off-centered loading.

### MDENT Finite Element Models

Three-dimensional FEM's of the MDENT, MDENT-2, and MDENT-3 geometries were created using 20-node reduced integration bricks. Two symmetry planes were utilized in creating the FEM's by dividing the geometry along the longitudinal axis and along the center of the notch root. A concentrated force was applied to a node or nodes along the top of the "pin hole" to simulate centered or off-centered loading. In addition, a 3-D FEM of the MDENT-3 with a crack located in one notch root was created using the multi-step processed described for the 3-D cracked separation bolt model. The 3-D cracked FEM consisted of 17,032 20-node reduced integration bricks and 79,129 nodes, and the FEM is illustrated in Figure 7.

## FINITE ELEMENT RESULTS

### Stress Field Comparisons

Axial stress across the notch section of the separation bolt at proof load is compared to axial stress across the notch section for the NP at an equivalent load in Figure 8. The equivalent load was based on a cross sectional area ratio, and the NP stress values are taken along the symmetry plane at the center of the NP specimen geometry. Notched plate stress values are plotted for the case of the load centered on the NP land and for two cases where the load is offset ±0.0521 in. on the land.

The offset distance of 0.0521 in. represents an offset of approximately one-quarter land width and was chosen as a matter of convenience due to FEM node spacing. The centered NP load case slightly overestimates the axial stress in the vicinity of the notch but predicts a significant compressive stress on the backface of the section. The case with the load offset toward the notch over-predicts the axial stress for approximately 70% of the notch section and then produces a very large compressive stress on the backface, indicating a significant bending load on the notch section. The case with the load offset toward the backface slightly underestimates the separation bolt stress profile, but does not predict a compressive stress on the backface.

The axial stress across the separation bolt notch section at proof load is compared to the axial stress across the notch section in the three MDENT specimen geometries at an equivalent load in Figure 9. The equivalent load was based on a cross sectional area ratio, and the MDENT stress values are taken along the symmetry plane at the center of each MDENT specimen geometry. For each MDENT specimen the load application point is offset 0.0512 in. towards the "right" (as labeled in Figure 7) to simulate approximately one-quarter land width off-center loading. Stresses are then plotted for both the "left" and "right" notch sections. For all of the MDENT offset cases, the right notch stresses overestimate the bolt axial stresses and the left notch stresses underestimate the bolt stresses. The difference between the left and right notch stress predictions decreases significantly for the MDENT-3 specimen, verifying the effectiveness of the flexure section in reducing misalignment induced bending effects. The MDENT-3 specimen with centered load predicts stress distributions that essentially match the separation bolt stresses in the vicinity of the notch and that reasonably match the majority of the bolt stress distribution. All of the MDENT geometries predict varying amounts of compressive stress on the backface.

The effective (von Mises), axial, radial, and hoop stress profiles across the separation bolt notch section at proof load are compared to the corresponding stress values across the notch section of the MDENT-3 specimen at an equivalent load in Figure 10. For this case, the equivalent load for the MDENT-3 was scaled to approximately match the plastic zone size in the notch region. Therefore, the effective stress predictions and corresponding plastic zone sizes are very similar for the separation bolt and the MDENT-3. The MDENT-3 underpredicts the peak axial stress in the bolt by approximately 3% and predicts a compressive axial stress on the backface. The radial stress predictions for the bolt and MDENT-3 are almost identical. The MDENT-3 significantly underestimates the hoop stress in the bolt due to the lack of hoop constraint inherent in the MDENT-3 geometry.

## Crack Results

Figure 11 shows the variation of $J$ along the crack front for the separation bolt at proof and flight load and for the MDENT-3 specimen at the same equivalent load presented in the Figure 10 results. The results shown in Figure 11 are for a crack in the notch root with crack dimensions of $a = c = 0.125$ in., where $a$ is crack depth and $c$ is one-half crack length. The predicted $J$ distributions for the MDENT-3 closely match the proof load and flight load separation bolt $J$ distributions.

The crack front constraint condition for different geometries can be quantified using the non-dimensional parameter $\beta$ defined as

$$\beta = \frac{T\sqrt{\pi a}}{K_I} \tag{1}$$

where $T$ is the elastic $T$-stress, a is the crack depth, and $K_I$ is the mode I stress intensity factor.[5] Figure 12 shows the variation of $\beta$ along the crack front for the separation bolt and for the MDENT-3 specimen with crack dimensions of $a = c = 0.125$ in. The $\beta$ values for several standard fracture test specimens are also plotted.[5] The $\beta$ values for the MDENT-3 specimen are similar to the separation bolt values, thus demonstrating a comparable crack front constraint condition for the two geometries.

## CONCLUSIONS

In summary, four test specimen configurations were analyzed in an attempt to match the elastic-plastic stress field and crack constraint conditions present in the separation bolt. Of the four test specimens analyzed, the MDENT-3 most closely approximates the stress field, $J$ values, and crack constraint conditions found in the flight hardware. The MDENT-3 is also most insensitive to load misalignment and/or load redistribution during crack growth.

**Table 1. General Material Properties for 4340 Steel**

| | |
|---|---|
| Elastic Modulus, $E$ (psi) | $30\times10^6$ |
| Poisson's Ratio, $\nu$ | 0.29 |
| Tensile Yield Strength, $F_{ty}$ (psi) | $180\times10^3$ |
| Tensile Ultimate Strength, $F_{tu}$ (psi) | $198\times10^3$ |

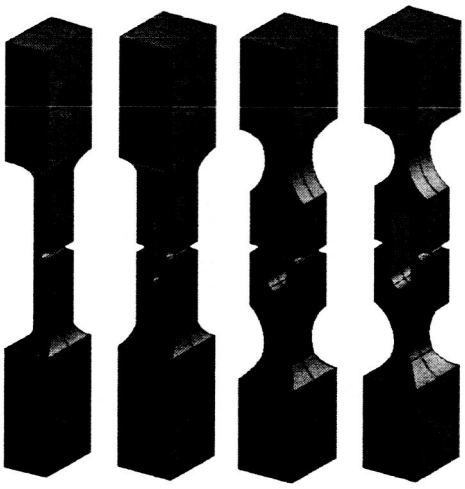

(a) (b) (c) (d)

**Figure 1. Illustration of: (a) Notched Plate , (b) MDENT, (c) MDENT-2, (d) MDENT-3**

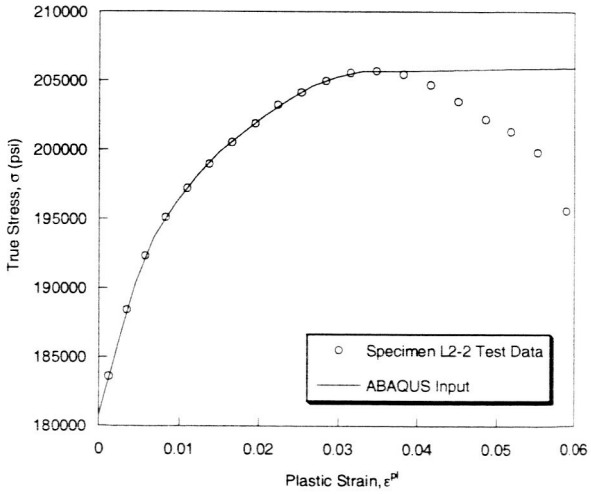


**Figure 2. ABAQUS FEM Plasticity Inputs Compared to Uniaxial Tensile Test Data**

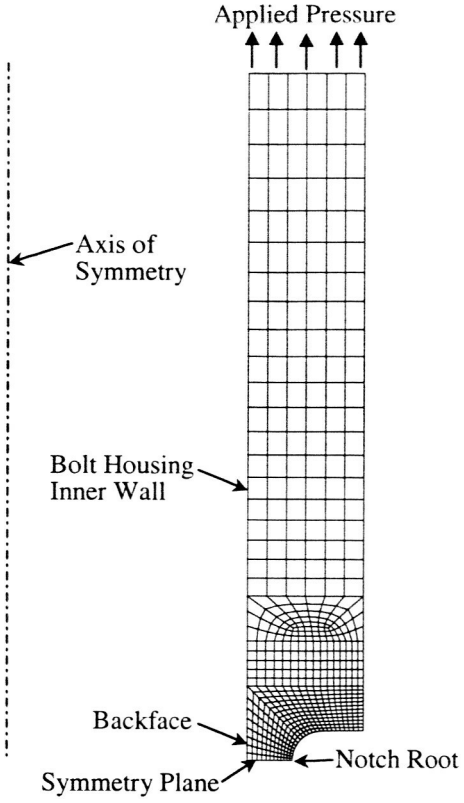


**Figure 3. Axisymmetric FEM of Separation Bolt**

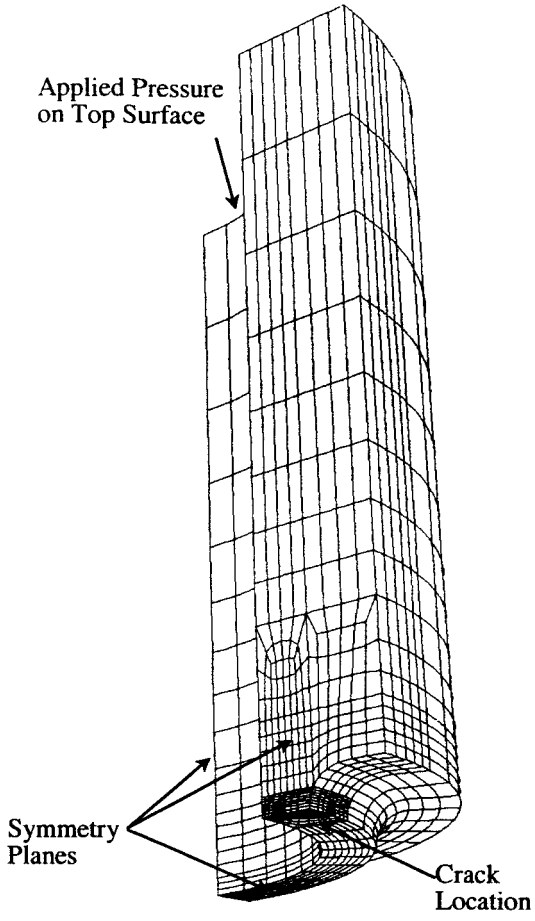


**Figure 4. 3-D FEM of Separation Bolt with Crack in Notch Root**

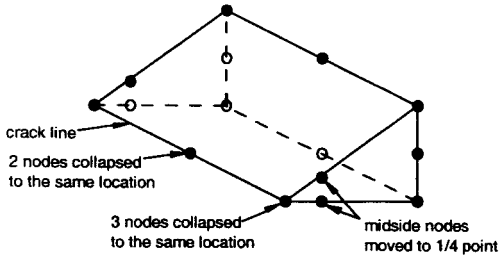


**Figure 5. 20-Node Brick Element with a Collapsed Face to Create Singular Fields**

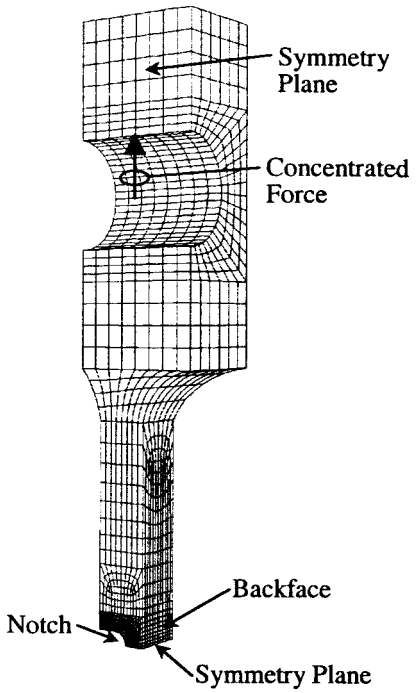


**Figure 6. 3-D FEM of Notched Plate Specimen**

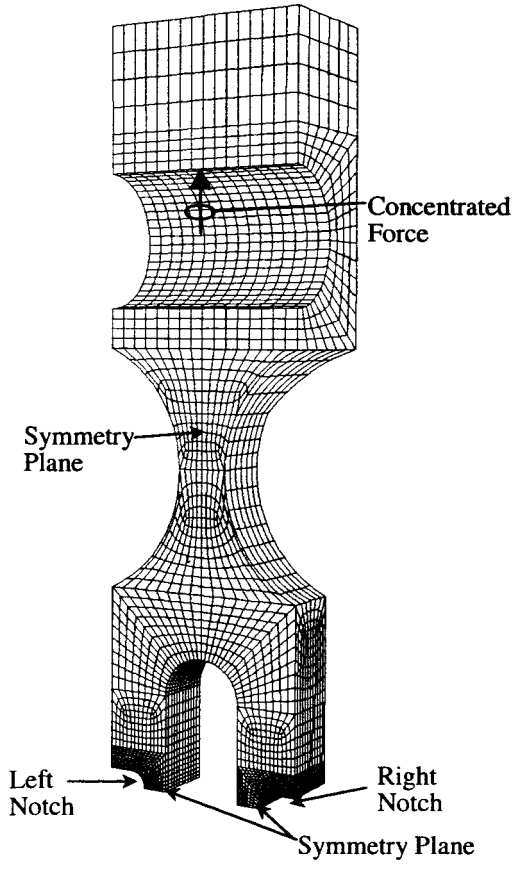


**Figure 7. 3-D FEM of MDENT-3 with Crack in Notch Root**

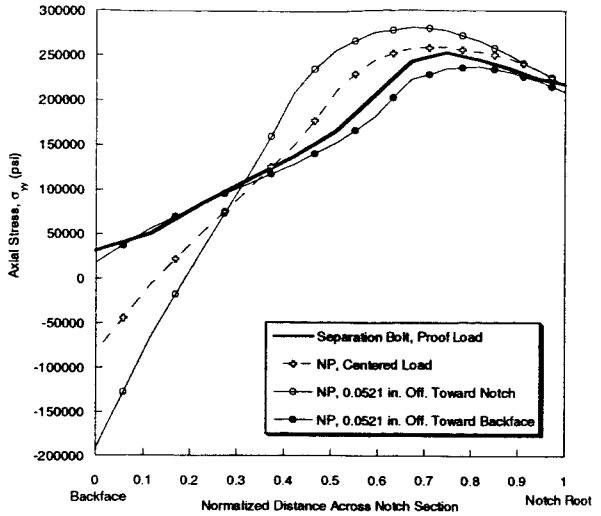


**Figure 8. Axial Stress Across the Notch Section of the Separation Bolt and the NP Geometry**

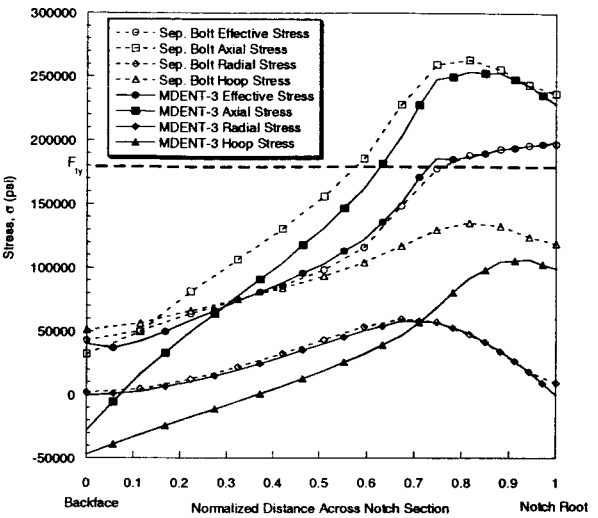


**Figure 10. Comparison of Stress Components Across the Notch Section for the Separation Bolt and the MDENT-3 Specimen**

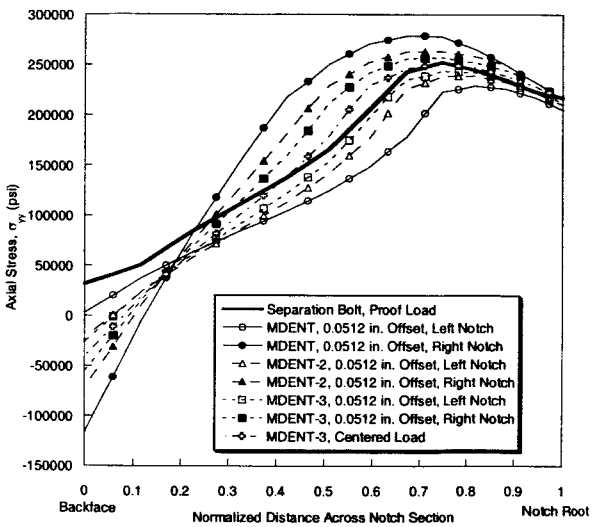


**Figure 9. Axial Stress Across the Notch Section of the Separation Bolt and Three MDENT Geometries**

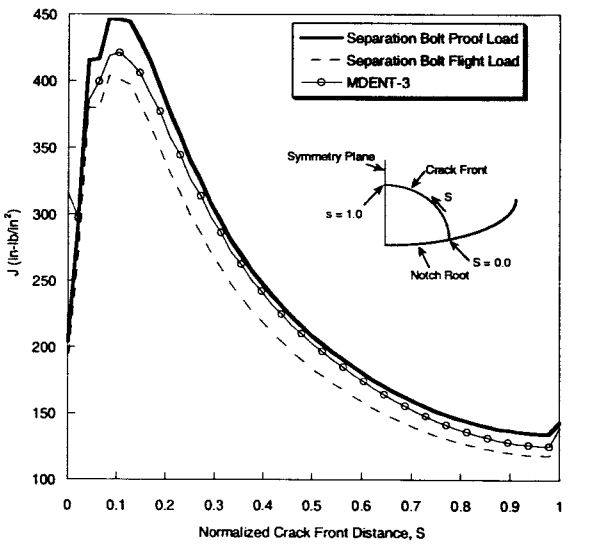


**Figure 11. Comparison of *J* Along the Crack Front for the Separation Bolt and the MDENT-3 Specimen**

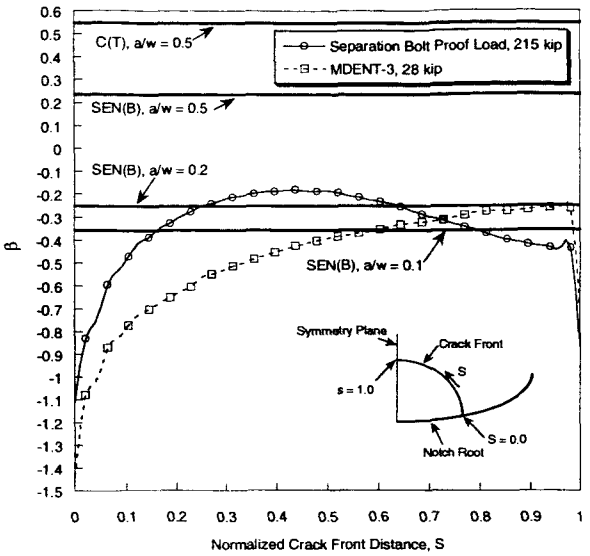


**Figure 12. Comparison of $\beta$ Along the Crack Front for the Separation Bolt and the MDENT-3 Specimen**

## REFERENCES


1. Forman, Royce and R.C. McClung, "NASGRO 4.0, Fracture Mechanics and Fatigue Crack Growth Analysis Software, Reference Manual," Southwest Research Institute, 2002.

2. ABAQUS Standard User's Manual, Version 6.3, Hibbit, Karlsson, and Sorensen, Inc., 2002.

3. Patran Users Manual, Version 9.0, MSC Software Corporation, 2000.

4. FEA-Crack User's Manual, Version 2.5, Structural Reliability Technology.

5. Sherry, A.H., C.C. France, and M.R. Goldthorpe, "Compendium of T-Stress Solutions for Two and Three Dimensional Cracked Geometries," Fatigue and Fracture of Engineering Materials and Structures, Volume 18, No. 1, 1999, pp141-155.